Eur. Phys. J. B **27**, 111–118 (2002)
DOI: 10.1140/epjb/e20020135

THE EUROPEAN PHYSICAL JOURNAL B
EDP Sciences

Electron diffraction and microscopy of single-wall carbon nanotube bundles produced by different methods

J.-F. Colomer[1,a], L. Henrard[2], Ph. Lambin[2], and G. Van Tendeloo[1]

[1] EMAT, University of Antwerp (RUCA), Groenenborgerlaan 171, 2020 Antwerp, Belgium
[2] Laboratoire de Physique du Solide, FUNDP, 61 rue de Bruxelles, 5000 Namur, Belgium

Received 8 August 2001 and Received in final form 14 March 2002

Abstract. The atomic structure of single-wall carbon nanotube bundles produced by three different techniques (laser ablation, electric arc discharge and catalytic chemical vapor deposition (CCVD)) has been characterized by electron diffraction and microscopy. Information on the helicity and the lattice packing has been obtained. Concerning the helicity, small bundles produced by CCVD exhibit only one or two tube helicities within a single bundle. The diffraction patterns of laser-ablation produced bundles also present well-defined but more diversified chiralities within a single bundle. By contrast the data acquired on bundles formed by arc discharge show a more diffuse pattern, characteristic of a random chirality dispersion within a single bundle. Concerning the lattice packing, informations are obtained *via* a detailed study of the equatorial line of the diffraction pattern for bundles produced by the three techniques. This electron diffraction study is completed by high-resolution electron microscopy.

PACS. 61.14.-x Electron diffraction and scattering – 68.37.Lp Transmission electron microscopy (TEM) (including STEM, HRTEM, etc.) – 61.48.+c Fullerenes and fullerene-related materials

1 Introduction

Since the discovery of carbon nanotubes by Iijima [1], extensive research has been devoted to their structural characterization [2]. The intrinsic simplicity of the single-wall carbon nanotubes (SWNTs) makes them ideal objects for the investigation of reduced dimensionality effects. Indeed, a single-wall carbon nanotube can be built by rolling up a single graphene sheet and is uniquely defined by its chiral vector $\mathbf{C}_{n,m} = n\boldsymbol{a}+m\boldsymbol{b}$, where $\boldsymbol{a}$ and $\boldsymbol{b}$ are the unit vectors of the honeycomb network, and n and m are integers [3]. Depending on the wrapping indices (n, m), different types of nanotubes are obtained: (1) zigzag nanotubes correspond to $(n, 0)$ and have a chiral angle of 0°, (2) (n, n) armchair nanotubes have a chiral angle of 30°, (3) other, chiral (n, m) nanotubes have a chiral angle ranging from 0° to 30°.

There are not so many techniques available today to fully characterize SWNT bundles. Global investigations can be done using methods applicable to macroscopic samples, such as Raman spectroscopy [4] and X-ray or neutron diffractions [5]. However, to study individual bundles (diameter, helicity, etc.), the only two powerful techniques are scanning tunneling microscopy (STM) [6–8] and transmission electron microcospy (TEM) coupled with electron diffraction (ED) [9]. The (n, m) identification is possible using STM images of atomically resolved isolated single-wall carbon nanotubes [6–8]. ED is the most direct and fast technique that gives access to detailed information about the structures of SWNTs within bundles [9].

Single-wall carbon nanotubes synthesized by three different methods (laser ablation, electric arc discharge and CCVD) have already been characterized by TEM techniques. Nanotubes appear sometimes isolated, but are most often packed together by van der Waals forces to constitute bundles [9]. Concerning the laser ablation method [10], high-resolution electron microscopy (HREM) and X-ray diffraction of the bundle material suggest that the individual single-wall nanotubes have a rather uniform diameter of approximatively 13.8 Å in typical conditions and are ten to hundred micrometer long. They are packed within the ropes in a two-dimensional triangular lattice with van der Waals inter-tube bonding (estimated to be 3.2 Å) and lattice constant equal to 17 Å, typically. Another popular technique for the production of SWNTs is the electric arc discharge. A great similarity in the characteristics of SWNT samples has been found with those produced by laser ablation [11]. Indeed, the SWNTs have diameters around 14 Å, and they form crystalline bundles of a few tens of tubes. The atomic structure (*i.e.* diameter) of the SWNTs synthesized by these two techniques depends on the growth conditions (temperature, catalysts, etc.) [12,13].

The SWNTs produced by the CCVD method show a structural organization different from those synthesized by

[a] e-mail: jfcolom@ruca.ua.ac.be

the first two techniques. Samples constitute of SWNTs organized in bundles, mixed with isolated SWNTs present in large quantity [14,15]. The diameter distribution of SWNTs appears to be large (between 8 and 20 Å) [15].

Electron diffraction is a technique well-suited to characterize carbon nanotubes. It was first proved for the case of multi-wall nanotubes, for which the chiral character of the structure has been analysed [1]. ED has also been applied to single-wall carbon nanotubes [9] and various works have been performed to determine the helicity of SWNTs within the bundles[16–24]. A nanodiffraction study [16] obtained on a sample produced by laser ablation showed that the SWNTs present a predominant helicity corresponding to the armchair (10,10) tubes, together with a small proportion of (11,9) and (12,8) tubes, as previously predicted [10]. However other results using nanodiffraction [17] or selected-area electron diffraction (SAED) [18,19] revealed a wide range of helicities. In most cases, the helicity was found to be randomly distributed in the range between the zigzag and armchair structures [17–21]. As for the SWNTs synthesized by electric arc discharge, detailed SAED experiments indicated a uniform distribution of helicity in the bundles [22]. Concerning the SWNTs produced by the CCVD method, we have already reported that the smallest bundles of SWNTs most often exhibit a well-defined helicity, due to a small number of tubes within the bundle, but no preferred helicity has been found [23]. Very recently, new results showed that the synthesis of perfectly ordered single crystals of SWNTs with identical diameters and chiralities is possible using thermolysis of nano-patterned precursors [24].

In this paper, we present new and detailed experimental results obtained by electron diffraction on small and isolated straight bundles of single-wall carbon nanotubes produced by the three aforementioned methods of production. Comparing for the first time SWNT bundles produced by different techniques under the same experimental conditions, we were able to confirm that the small bundles produced by the CCVD method exhibit only one or two tube helicities within a single bundle. The diffraction patterns of bundles produced by laser ablation also present well-defined but multiple helicities within well crystalline bundles. The data acquired with arc-discharge produced bundles however give more diffuse patterns, associated with a wider distribution of helicities within a single bundle. Moreover, for the first time, we obtain and compare informations about the lattice packing of the bundles produced by the three different methods by analysing the equatorial line of diffraction patterns. This study is completed by a HREM characterization of SWNT material used in the ED experiments.

2 Experimental

Laser ablation SWNT samples were produced as described in [10]. The SWNTs synthesized by electric arc discharge were produced with a mixture of Ni/Y/99 at % following the procedure described in [11]. The CCVD SWNTs were synthesized on 2.5 wt % Co/MgO catalyst by decomposition of methane at 1000 °C and purified by a hydrochloric acid treatment to remove the catalyst. The experimental procedure has been reported in [14].

The tube-containing material was mechanically transferred to a copper transmission electron microscope grid and examined in a JEOL 200 CX microscope.

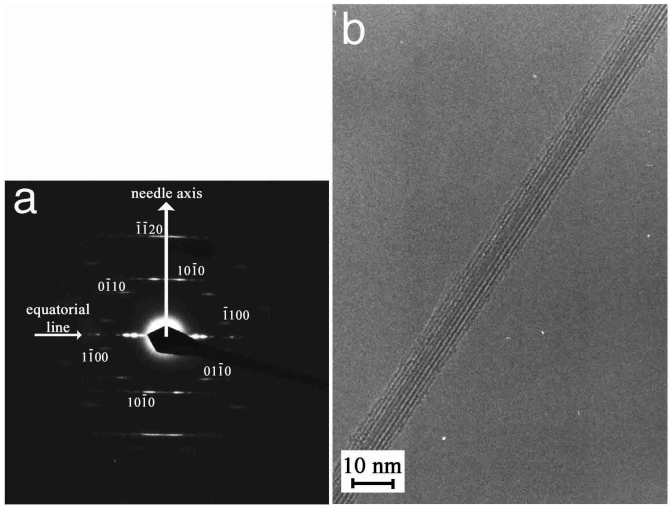

Fig. 1. (a) Selected area electron diffraction pattern of a bundle synthesized by the CCVD method at normal incidence and (b) TEM image of the bundle involved in the ED experiment.

3 Results and discussion

We focus our ED study on isolated straight bundles of SWNTs produced by the three methods mentioned above. We start with bundles produced by the CCVD method [14]. Figure 1a displays a typical ED pattern obtained at normal incidence on a single straight bundle. The two main features in the ED pattern is a line crossing the central 000 beam which is perpendicular to the bundle axis (equatorial line) and the $hk.0$ reflections situated on two concentric "circles" centred on the 000 beam. The radii of the inner and outer circles are consistent with the length of the diffraction vectors of type $10\bar{1}0$ and $11\bar{2}0$ of graphite, respectively. Both $10\bar{1}0$ spots and $11\bar{2}0$ spots form perfect hexagons on the two circles. There are two hexagons by around each circle suggesting the presence of a single helicity for a chiral tube. The orientation of the two hexagons in the same circle differs by an angular separation of 2α (experimental angle) where α is the chiral angle. A detailed theoretical analysis of such pattern has been provided within the reciprocal space description of carbon nanotubes [2,25,26] or by the kinematical theory of electron diffraction [27–29]. In the present case, the experimental angle has been estimated around 32°; the chiral angle α is therefore 16°. A precise measurement of the angle is made difficult by the streaking of the spots due to the strong curvature of the (tubes) bundle.

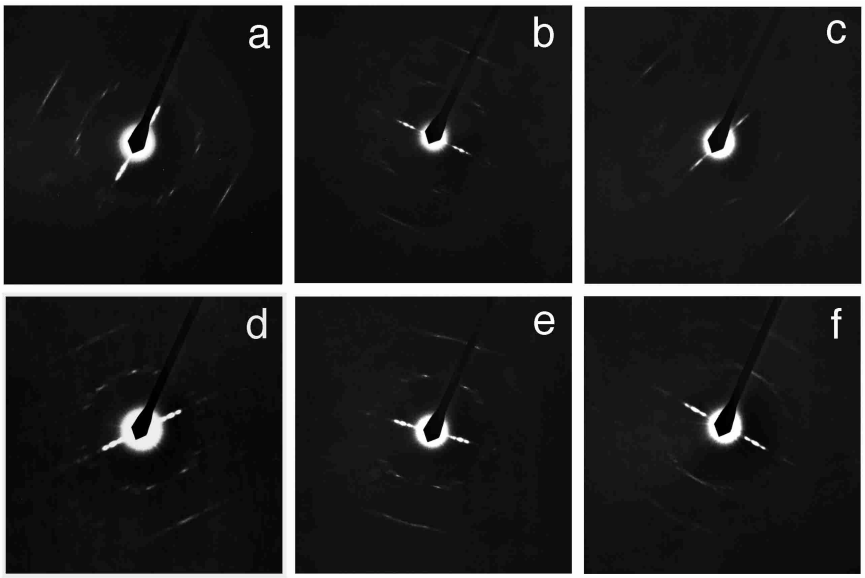

Fig. 2. Selected area electron diffraction patterns of SWNT bundles synthesized by the CCVD method at normal incidence showing one helicity (a) 25°, (b) 24°, and (c) 30°, or two helicities (d) 16° and 27°, (e) 20° and 26°, or (f) more than two.

Considering the equatorial line, the spot positions along this line are determined by the stacking periodicity of the tubes and the orientation of the bundle with respect to the electron beam. The detailed analysis of the equatorial line will be given after the discussion about the observed helicities.

A TEM image of the SWNT bundle involved in the ED experiment is given in the Figure 1b. In this case, the bundle has 8 nm in diameter and is not twisted along the needle axis. Generally, we have chosen the bundles that are not the result of a coalescence of other bundles. The average diameter of the bundles considered in the ED experiments was around 10 nm (20–30 tubes) and we estimated the average lattice parameter to be around 14 Å.

The ED experimental pattern displayed in Figure 1a is a typical example selected from a more systematic study. Other well-defined diffraction patterns obtained on bundles synthesized by the CCVD method have been recorded and some of them are shown in the Figure 2. The diffraction pattern contrasts have been adjusted to optimize the analysis of the *hk*.0 reflections. In the ED patterns, both the $10\bar{1}0$ spots whose positions contain all the information about the helicity of the SWNTs and the equatorial line that gives informations about the packing are well visible. Generally, when we observe well-defined helicities in the diffraction pattern, the corresponding equatorial line presents well-defined spots as well, *i.e.* the crystallinity of the bundle is good. In all the diffraction patterns shown in the Figure 2, the helical angles can be estimated. These patterns confirm the fact that most of the small bundles produced by the CCVD method exhibit only one or two tube helicities [23]. Among 20 diffraction patterns from small SWNT bundles recorded in this work, 9 revealed a single helicity and 8 were found with two helicities. In the case of patterns having just one helicity, the helical angles are often close to 30° (Figs. 2a to c). When two chiralities are observed, the helicity distribution seems to be broader (Figs. 2d and e). The exact chiral angles are given in the caption of the Figure 2. The last diffraction pattern (Fig. 2f) presents several helicities (more than two) but the $10\bar{1}0$ circle remains clearly spotty. Except for a weak tendency for the "armchair structure" when the bundles present a single helicity, no preferred helicity was found. We have already argued [23] that the small diameter of the bundles considered in the ED experiments in the case of SWNTs produced by the CCVD method seems to be the main reason for the selectivity of helicity. The observation of several helicities is attributed to the branching of several homogeneous bundles. This conclusion has also been substantiated by the fact that the equatorial line of CCVD bundles that exhibits 2 chiralities reveals two lattice parameters, *i.e.* the presence of 2 nanocrystals of different periodicity [23]. To complete this study, we now discuss in details two cases of intensity profile along the equatorial line for bundles presenting a single and two helicities, respectively. The first typical example of a spotty equatorial line is shown in Figure 3a, which is the magnification of the equatorial line of the diffraction pattern of Figure 1a exhibiting a single helicity ($\alpha = 16°$). Five spots can be distinguished and, in spite of their elongated shape, their spacing can be measured to estimate the bundle lattice parameter. The width of the peaks is due to the finite number of tubes in the bundles and the form factor of a single tube.

Figure 3b displays the experimental equatorial line profile of intensities. We observe that the signal intensity of several spots is saturated, giving an uncertainly on their positions. Figure 4 represents the equatorial line profile computed with the kinematical theory for a homogeneous bundle of nanotubes approximated by

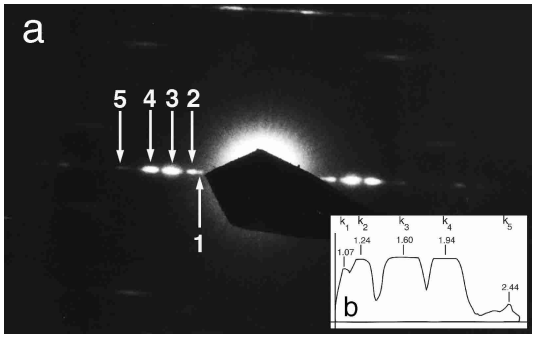

Fig. 3. (a) Magnification of the equatorial line of the SAED pattern of Figure 1a and (b) experimental equatorial line profile of intensities.

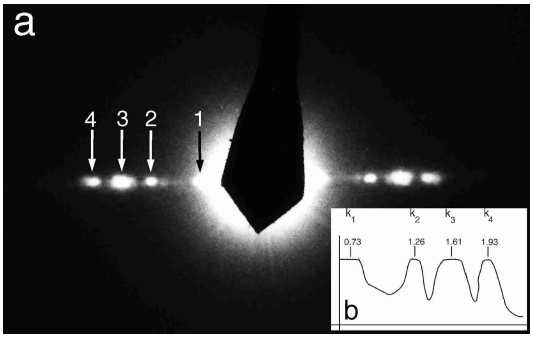

Fig. 5. (a) Magnification of the equatorial line of the SAED pattern of Figure 2e and (b) experimental equatorial line profile of intensities.

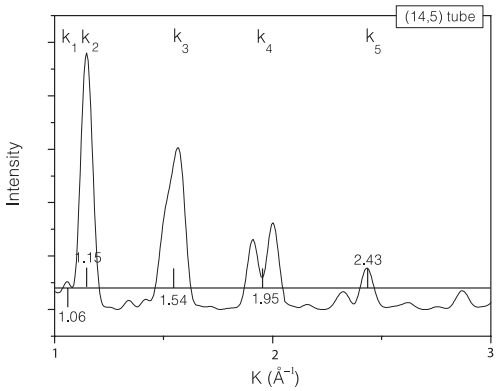

Fig. 4. Computed equatorial line profile for SWNT bundle made of (14,5) tubes. The horizontal line represents a possible saturation level of the spot in the experimental profile.

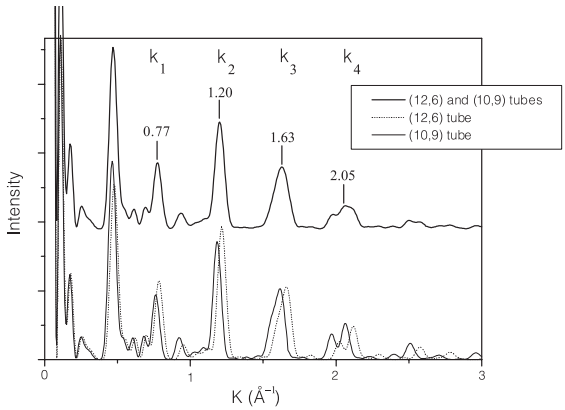

Fig. 6. Computed equatorial line profiles for SWNT bundles made of (12,6) and (10,9) tubes.

continuous cylinders [2,22,23] and composed of 31 (14,5) tubes ($d_t = 13.36$ Å). The comparison of the experimental diffraction profile (Fig. 3b) and the simulated curve (Fig. 4) indicates that the observed bundle could be constituted of (14,5) tubes.

The second analysis of a spotty equatorial line has been made for the bundle presenting two chiralities: 20 and 26° (the corresponding SAED pattern is given in Fig. 2e). Along the equatorial line (Fig. 5a), four spots can be distinguished. As for the precedent case, the experimental equatorial line profile of intensities has been drawn (Fig. 5b) showing that all the spot intensities are saturated in intensity.

Figure 6 represents three equatorial line profiles computed for two homogeneous bundles, one made of 31 (12,6) tubes ($d_t = 12.44$ Å, $\alpha = 19°$) and the other by 31 (10,9) tubes ($d_t = 12.89$ Å, $\alpha = 28°$); the third profile is the sum of the first two curves and describes the diffraction pattern that would result by combining the two nanobundles, constituted by the two types of tubes. Due to the similar diameter of the two types of tubes involved (12.44 and 12.89 Å), no definitive conclusion can be drawn for this equatorial line only: the bundle could be the result of the association of two monochiral nanobundles (one composed of tubes with chirality around 20° [(12,6) tubes] and another with chiral angle around 26° [(10,9) tubes]) with nearly the same diameter, as shown by the full line in Figure 6. Or the bundle could be made of a mixing of both kinds of tube within a single lattice. In both cases, there is reasonable correspondence between the experimental spot positions and the computed values. Note that in reference [23], we have shown a case where the equatorial line of a bundle have to be analysed in term of two distinct nanobundles with distinct lattice parameters.

Another observation concerns the lattice parameter extracted from this detailed analysis of the equatorial line. Indeed, in the two cases studied, the tube diameters were around 12–13 Å (depending on the considered case) involving a lattice parameter around 16–17 Å. Based on the TEM images, we have already estimated the average lattice parameter in a series of bundles to be around 14 Å. This difference can be explained by the dispersity of diameters of the SWNTs synthesized by the CCVD method [15] where the diameter distribution appears larger than in the samples produced by other methods. Note that in the previous paper [23], the value of the lattice parameter extracted from a similar study corresponded precisely to the average 14 Å.

For the laser production, previous SAED studies [18,19] revealed an uniform distribution of the helicities in the SWNT bundles. The corresponding diffraction patterns show continuous intensity arcs on the $10\bar{1}0$ and

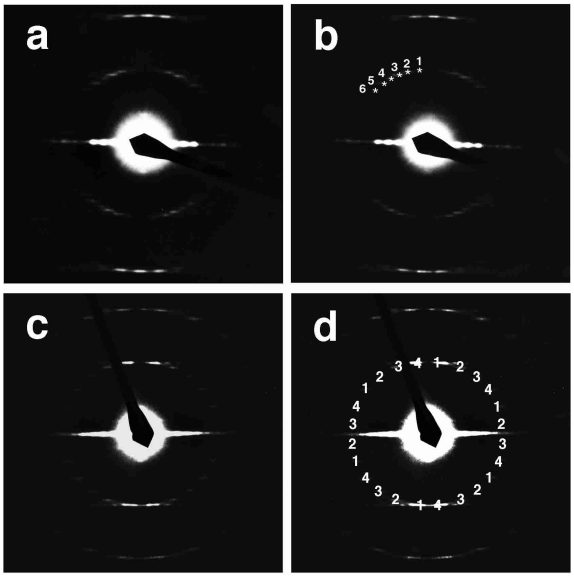

Fig. 7. Selected area electron diffraction patterns of SWNT bundles synthesized by laser ablation at normal incidence: (a) experimental pattern exhibiting three helicities and (b) the same pattern with the identification of the six hexagons, (c) other experimental pattern exhibiting two helicities and (d) the same pattern with the identification of the four sets of hexagons.

$11\bar{2}0$ diffraction circles, the reflection intensity being concentrated narrowly at the positions corresponding to the armchair structure [18,19].

Figure 7 displays two typical ED patterns of SWNTs produced by laser ablation. We do not observe the continuous intensity arcs, characteristic of a uniform helicity distribution. Instead, several clearly separated spots reveal the presence of multiple but well-defined helicities. The intensity of the spots is weaker near the equatorial line than close to the two poles and the spots are elongated in the direction normal to the tube axis, due to the curvature of the tubes and the finite size of the bundle. Both properties are in agreement with computer simulations [2].

Analyzing in detail the first experimental diffraction pattern (Fig. 7a), six hexagons can be seen. They have been visualized by numbering one of their vertices (Fig. 7b). They are grouped two by two and three angles 2α can be estimated to be 53°, 38° and 23°, corresponding to three chiral angles 26.5°, 19° and 11.5°. The second diffraction pattern is shown in Figure 7c. The inner circle contains four hexagons of weak, elongated spots, labelled from 1 to 4 in Figure 7d. The two hexagons, noted 2 and 3, correspond to a chiral structure with an angle 2α estimated around 45° corresponding to a chiral angle of 22.5°. The other two sets of hexagons, noted 1 and 4 give an angle 2α estimated around 18° corresponding to a chiral angle of 9°. A precise measurement of the angle 2α is made difficult by the streaking and the weak intensity of the spots.

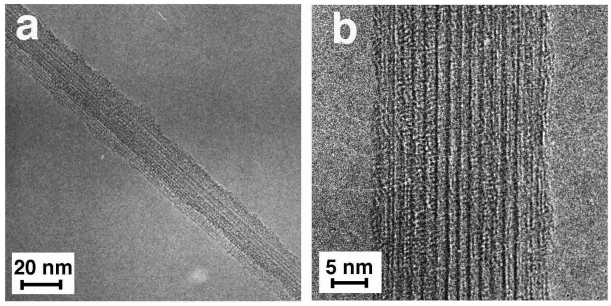

Fig. 8. Transmission electron microscopy images of SWNT bundles synthesized by laser ablation, the images a and b correspond to the diffraction patterns shown in Figure 7a and c, respectively.

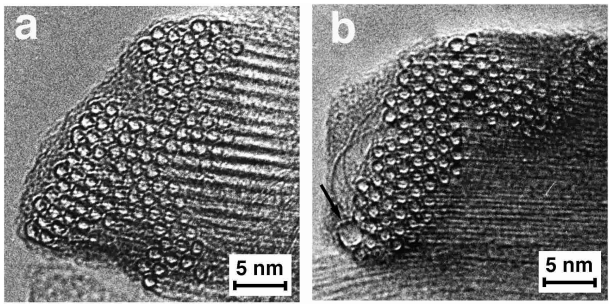

Fig. 9. "Cross section" of the bundles (tubes axis perpendicular to the image plane) showing a triangular lattice involving more than 100 tubes with (a) a lattice parameter of 17 Å and (b) a lattice parameter of 16.3 Å (the arrow marks a tube with a larger diameter). The tubes are produced by laser ablation technique.

Figure 8 shows the TEM images of the SWNT bundles used in the ED experiments described above. However, the bundles appear to be straight and the tubes are perfectly aligned, with no twisting or bending of the bundle. The inter-fringe distance depends on the orientation of the triangular lattice with respect to the electron beam and this distance is constant all over the image. We estimate the bundle diameters involved to 20 nm (Fig. 8a) and 23 nm (Fig. 8b).

Figure 9a shows a "cross-section" view of a $\sim$ 100-tube bundle oriented with its axis parallel to the beam direction. This figure reveals clear close-packed triangular arrangements that appear to be perfect. The SWNTs are fairly uniform in diameter as far as it can be determined by HREM. The two-dimensional triangular lattice has a lattice constant of 17 Å. Assuming an inter-tube distance of 3.2 Å, the mean tube diameter is 13.8 Å. The HREM images of the SWNT bundles (generally) agree well with the data reported previously [10]. However, slightly different tube diameters have also been found inside the same batch of samples, as *e.g.* in Figure 9b, where the lattice constant value is about 16.3 Å. Another observation in Figure 9b is the presence of one nanotube with a larger diameter (around 28 Å, indicated by the arrow) than the others (13.1 Å). Such significantly larger tubes are generally located in the external layers of the bundle.

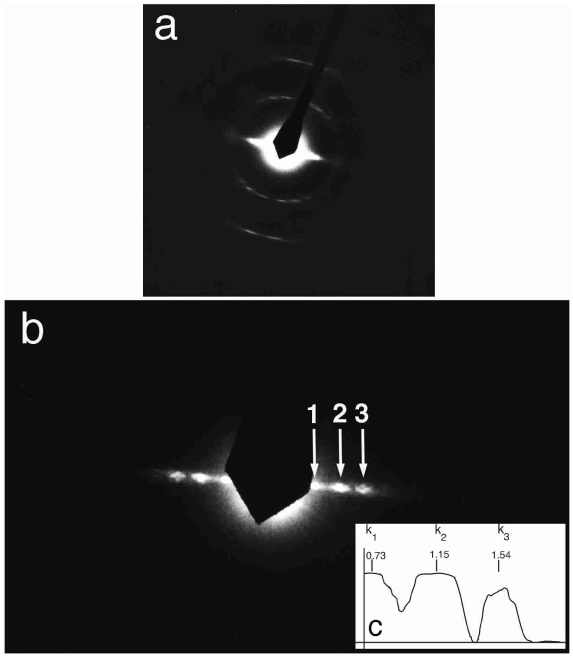

Fig. 10. (a) Selected area electron diffraction pattern of a bundle synthesized by laser ablation at normal incidence exhibiting two helicities (18° and 30°). (b) Magnification of the equatorial line and (c) Intensity along the equatorial line.

A striking feature in such sectional views is that typical bundles of SWNTs in our sample appear to be made of several smaller, well-defined nanocrystalline bundles. Having that in mind, it is tempting to attribute the few helicities observed by ED to separated nanobundles. We also note that the bundles chosen have a larger diameter than the ones we have considered for the SWNTs produced by CCVD. With the laser-produced nanotubes, it was very difficult to find bundles with small diameter due to the strong coalescence of the bundles in ropes. We believe that this is why the bundles generally present a distribution of helicities due to the coalescence of smaller bundles. And for the smaller ones, we found well-defined but multiple helicities can be observed. This fact is consistent with the hypothesis already given for the SWNTs produced by CCVD where the larger bundles appear to be the result of the coalescence of smaller ones with different helicities and diameters.

For the sake of comparison, we analyze the equatorial line of a bundle exhibiting defined helicities produced by laser ablation. The corresponding diffraction pattern is given in Figure 10a. Along the first circle of diffraction, three elongated spots can be observed on both sides of the north and the south poles. One set of spots, the weaker ones, corresponds to the armchair structure ($\alpha = 30°$), and the two others, to a chiral structure with an angle 2α around 36° and, then, a chiral angle α of 18°. In the corresponding experimental equatorial line (Fig. 10b), three intense spots come out and their spacing can be measured to estimate the bundle lattice parameter. Figure 10c displays the experimental equatorial line profile with the estimated positions of the spots.

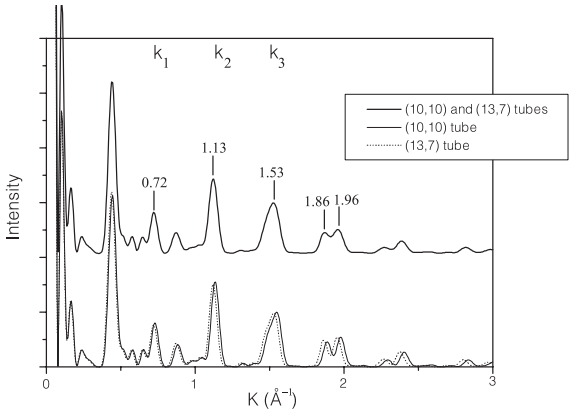

Fig. 11. Computed equatorial line profiles for SWNT bundles made of (10,10) and (13,7) tubes.

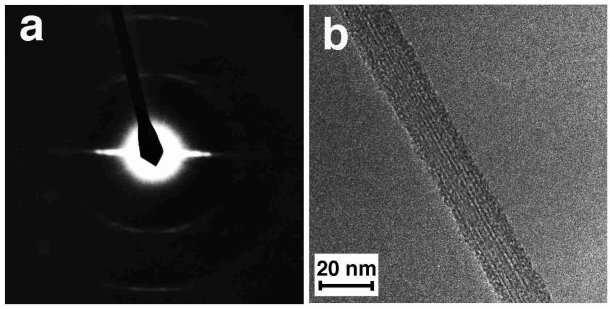

Fig. 12. (a) Selected area electron diffraction pattern of a bundle synthesized by electric arc discharge at normal incidence and (b) TEM image of the same bundle.

Figure 11 represents three equatorial line profiles computed for two homogeneous bundles, one made by 31 (13,7) tubes (d_t = 13.77 Å, $\alpha = 20°$) and the other by 31(10,10) tubes (d_t = 13.57 Å, $\alpha = 30°$); the third profile is the sum of the first two curves combining two nanobundles, one made of (13,7) tubes and the other made of (10,10) tubes. In this case, as for Figure 6, definitive conclusions can not be drawn from the comparison of Figure 10b and Figure 11 on the formation of the considered bundle from this analysis of the equatorial line, due to the similar diameter of the two types of tubes.

We now focus our attention to the SWNTs produced by electric arc discharge. Detailed SAED experiments have already been done and show a uniform distribution of helicity in the bundles [22]. The SWNT bundles generally contain 20 or 30 tubes, with a diameter ranging from 5 to 20 nm, *i.e.* they are generally smaller than the ones synthesized by laser ablation.

Figure 12a displays a typical ED pattern obtained on a SWNT bundle synthesized by electric arc discharge. The isolated SWNT bundle observed in the ED experiment appears straight with no twisting or bending (Fig. 12b); its diameter is 17 nm. Focusing our interest on the helicity, the main feature observed in the experimental diffraction pattern is the presence of two diffuse arcs located around the $10\bar{1}0$ and $11\bar{2}0$ diffraction circles. The diffracted intensity along these arcs is not as spotty as it was in the

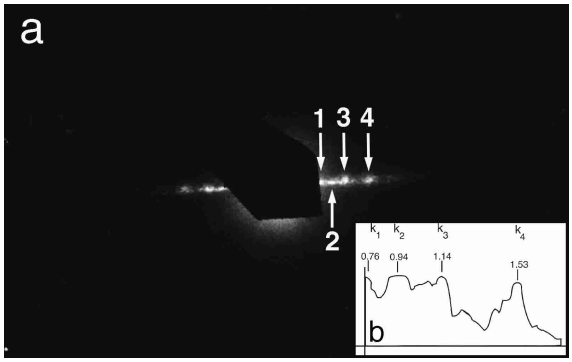

Fig. 13. (a) Magnification of the equatorial line of the SAED pattern for a bundle exhibiting a distribution of chiralities and (b) experimental equatorial line profile of intensities.

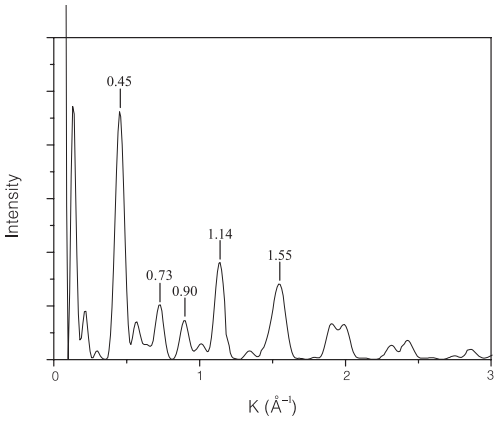

Fig. 14. Computed equatorial line profile for a bundle exhibiting a distribution of chiralities (mean diameter of tubes equal to 13.6 Å).

previous cases for SWNTs produced by CCVD or laser ablation. The largest intensity is found near the north and south poles, and a weaker one near the equator. This diffuse distribution of intensity has already been explained by the presence of a random and continuous distribution of helicities [22]. Concerning the equatorial line of this ED pattern, it appears diffuse and without clear maxima due to the strong diffracted intensity along this line. Then, to complete the study, we have adjusted the contrast of the diffraction patterns to optimize the observations of the spots along this line for the very same bundle. Along the line (Fig. 13a), four spots can be distinguished and their spacing can be measured to estimate the bundle lattice parameter. Figure 13b displays the experimental equatorial line profile of intensities with the estimated positions of the spots. Figure 14 represents the equatorial line profiles computed for a bundle presenting a large distribution of helicities (mean diameter of tubes equal to 13.6 Å). There is a fair agreement with the peak positions measured experimentally.

Another but atypical diffraction pattern is shown in Figure 15. The pattern contrast results from a longer exposure time used to reveal the *hk*.0 reflections, which explains why the 000 spot appears so large. In this case,

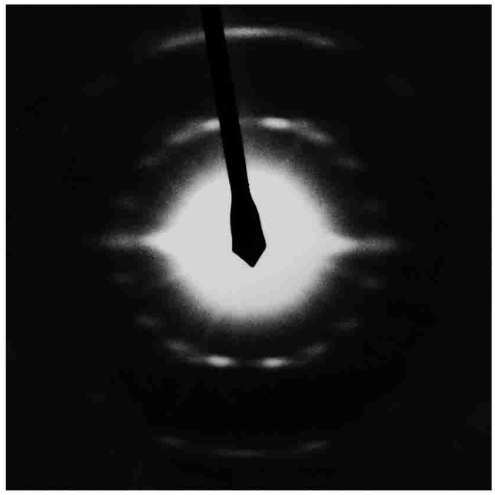

Fig. 15. Selected area electron diffraction pattern of a SWNT bundle synthesized by electric arc discharge at normal incidence.

the $10\bar{1}0$ diffraction circle is spotty, but the spots are diffuse. The long exposure time explains the diffuse character of the $10\bar{1}0$ spots. However, the distribution of helicities is not continuous as in the previous case, but localised around precise angle values. Unfortunately, information on the packing of the tubes inside the bundle is impossible to deduce from the structure of the equatorial line due to the very broad 000 spot.

The results obtained from bundles synthesized by electric arc discharge are consistent with the previous studies [22]. We never found in the sample a bundle having precise helicities such as in the samples produced by the CCVD method or laser ablation, even in the cases where the bundle diameter was very small. This fact might be explained by a wider dispersion of the tube diameters within a single bundle.

As a last comment, we would like to emphasize the differences in the equatorial line of diffraction between CCVD bundles and bundles produced by other methods (laser ablation, electric arc discharge). For electric arc discharge and laser ablation, only three or four spots (for $k \leq 1.50$ Å^{-1}) are observable whereas for CCVD bundles peaks up to 2 Å have been resolved.

Generally, the computed line profiles (Figs. 11 and 14) reproduce well the intensities of the laser ablation and electric arc discharge bundles but not the intensities of the CCVD bundles, even if one takes into account the non linear response of the photographic film. In particular, the intensity of spots around 2 Å^{-1} is most often underestimated by the simulation made within the continuum model. First, an average on all the cristallographic orientations of the bundle with respect to the electron beam has been performed in order to simulate the twist of the bundle. Indeed, this effect changes the orientation of the bundle lattice with respect to the electron beam. However, inside the selected-area used in the ED experiments, the considered bundle may not present all possible cristallographic orientations, when the twist period is too large.

As consequence, the intensity profile of the equatorial line can not be completely described by the simulations. Second, nanotubes represented by continuous cylinders were considered in the present simulation. A carbon-carbon coherent atomic packing inside the bundle might influence the intensity of the peaks. A more complete study about the intensity profile along the equatorial line based on the kinematical theory of diffraction is in progress [30].

4 Conclusion

We have performed a detailed electron diffraction analysis of SWNT bundles synthesized by the three common production methods of, *i.e.* the catalytic chemical vapor deposition, laser ablation and electric arc discharge. This analysis has been completed by an HREM characterization of the bundles. We confirm that most of the small bundles produced by the CCVD method exhibit one or two helicities. In the case of laser ablation, well-defined helicities are also found for bundles with small diameters. We attribute the distribution of helicities to the coalescence of small bundles to constitute larger bundles. For the SWNTs produced by electric arc discharge, we find a distribution of helicities for the small bundles that could be explained by the non- uniform diameter of tubes within a single bundle. Moreover, a peak with abnormal high intensity at $k \approx 2$ Å^{-1} is found on the equatorial line of CCVD produced nanotubes.

The authors are grateful to the Belgian Inter-university Project on Reduced-Dimensionality Systems (PAI P4/10). L.H. is supported by the Belgian FNRS. The authors thank Dr C. Journet and P. Bernier (GDPC, Montpellier) and Dr D.T. Colbert (Rice University) for the SWNT samples produced by electric arc discharge and laser ablation. They also thank Prof. J.B. Nagy (FUNDP, Namur) to have allowed the production of SWNT samples by the CCVD method.

References

1. S. Iijima, Nature **354**, 56 (1991).
2. S. Amelinckx, A. Lucas, Ph. Lambin, Rep. Prog. Phys. **62**, 1471 (1999).
3. N. Hamada, S.I. Sawada, A. Oshiyama, Phys. Rev. Lett. **68**, 1579 (1992).
4. M.S. Dresselhaus, P.C. Eklund, Adv. Phys. **49**, 705 (2000).
5. S. Rols, R. Almairac, L. Henrard, E. Anglaret, J.-L. Sauvajol, Eur. Phys. J. B **10**, 263 (1999).
6. J.W.G. Wildoer, L.C. Venema, A.G. Rinzler, R.E. Smalley, C. Dekker, Nature **391**, 59 (1998).
7. T.W. Odom, J.L. Huang, Ph. Kim, Ch.M. Lieber, Nature **391**, 62 (1998).
8. L.C. Venema, V. Meunier, Ph. Lambin, C. Dekker, Phys. Rev. B **61**, 2991 (2001).
9. S. Iijima, T. Ichihashi, Nature **363**, 603 (1993).
10. A. Thess, R. Lee, P. Nikolaev, H. Dai, P. Petit, J. Robert, C. Xu, Y.H. Lee, S.G. Kim, A.G. Rinzler, D.T. Colbert, G.E. Scuseria, D. Tomanek, J.E. Fisher, R.E. Smalley, Science **273**, 483 (1996).
11. C. Journet, W.K. Maser, P. Bernier, A. Loiseau, M.L. De La Chapelle, S. Lefrant, P. Deniart, R. Lee, J.E. Fisher, Nature **388**, 756 (1997).
12. S. Bandow, S. Asaka, Y. Saito, A.M. Rao, L. Grigorian, E. Richter, P.C. Eklund, Phys. Rev. Lett. **80**, 3779 (1998).
13. C. Journet, Ph.D. Thesis, University of Montpellier (1998).
14. J.-F. Colomer, C. Stephan, S. Lefrant, G. Van Tendeloo, I. Willems, Z. Konya, A. Fonseca, Ch. Laurent, J.B. Nagy, Chem. Phys. Lett. **317**, 83 (2000).
15. J.-F. Colomer, J.-M. Benoit, C. Stephan, S. Lefrant, G. Van Tendeloo, J.B. Nagy, Chem. Phys. Lett. **345**, 11 (2001).
16. J.M. Cowley, P. Nikolaev, A. Thess, R.E. Smalley, Chem. Phys. Lett. **265**, 379 (1997).
17. H.Z. Jin, R.R. He, J. Zhu, J. Electron Microsc. **48**, 339 (1999).
18. D. Bernaerts, A. Zettl, N.G. Chopra, A. Thess, R.E. Smalley, Solid State Commun. **105**, 149 (1998).
19. L.C. Qin, S. Iijima, H. Kataura, Y. Maniwa, S. Suzuki, Y. Achiba, Chem. Phys. Lett. **268**, 101 (1997).
20. R.R. He, H.Z. Jin, J. Zhu, Y.J. Yan, X.H. Chen, Chem. Phys. Lett. **298**, 170 (1998).
21. J.M. Cowley, F.A. Sundell, Ultramicroscopy **68**, 1 (1997).
22. L. Henrard, A. Loiseau, C. Journet, P. Bernier, Eur. Phys. J. B **13**, 661 (2000).
23. J.-F. Colomer, L. Henrard, Ph. Lambin, G. Van Tendeloo, Phys. Rev. B **64**, 125425 (2001).
24. R.R. Schlittler, J.W. Seo, J.K. Gimzewski, C. Durkam, M.S.M. Saifullah, M.E. Welland, Science **292**, 1136 (2001).
25. X.B. Zhang, X.F. Zhang, S. Amelinckx, G. Van Tendeloo, J. Van Landuyt, Ultramicroscopy **54**, 237 (1993).
26. X.F. Zhang, X.B. Zhang, G. Van Tendeloo, S. Amelinckx, M. Op de Beek, J. Van Landuyt, J. Cryst. Growth **130**, 368 (1993).
27. L.C. Qin, J. Mater. Res. **9**, N °9, 2450 (1994).
28. A.A. Lucas, V. Bruyninckx, Ph. Lambin, Europhys. Lett. **35**, 355 (1996).
29. Ph. Lambin, A.A. Lucas, Phys. Rev. B **56**, 3571 (1997).
30. L. Henrard, J.-F. Colomer, G. Van Tendeloo, Ph. Lambin, in preparation.